7192 J. Med. Chem. 2010, 53, 7192–7201
DOI: 10.1021/jm100834y

Journal of Medicinal Chemistry Article

Surface Plasmon Resonance Biosensor Based Fragment Screening Using Acetylcholine Binding Protein Identifies Ligand Efficiency Hot Spots (LE Hot Spots) by Deconstruction of Nicotinic Acetylcholine Receptor α7 Ligands

Gerdien E. de Kloe,[†,#] Kim Retra,[‡,#] Matthis Geitmann,[§] Per Källblad,[§] Tariq Nahar,[⊥] René van Elk,[⊥] August B. Smit,[⊥] Jacqueline E. van Muijlwijk-Koezen,[†] Rob Leurs,[†] Hubertus Irth,[‡] U. Helena Danielson,[∥,§] and Iwan J. P. de Esch*[,†]

[†]*Leiden/Amsterdam Center for Drug Research (LACDR), Division of Medicinal Chemistry, Faculty of Sciences, VU University Amsterdam, De Boelelaan 1083, 1081 HV Amsterdam, The Netherlands,* [‡]*Leiden/Amsterdam Center for Drug Research (LACDR), Division of BioMolecular Analysis, Faculty of Sciences, VU University Amsterdam, De Boelelaan 1083, 1081 HV Amsterdam, The Netherlands,* [§]*Beactica AB, Box 567, SE-751 22 Uppsala, Sweden,* [∥]*Department of Biochemistry and Organic Chemistry, Uppsala University, BMC, Box 576, SE-751 23, Uppsala, Sweden, and* [⊥]*Department of Molecular and Cellular Neurobiology, Center for Neurogenomics and Cognitive Research, Neuroscience Campus Amsterdam, VU University Amsterdam, De Boelelaan 1085, 1081 HV, Amsterdam, The Netherlands.* [#] *These authors contributed equally.*

Received July 5, 2010

The soluble acetylcholine binding protein (AChBP) is a homologue of the ligand-binding domain of the nicotinic acetylcholine receptors (nAChR). To guide future fragment-screening using surface plasmon resonance (SPR) biosensor technology as a label-free, direct binding, biophysical screening assay, a focused fragment library was generated based on deconstruction of a set of α7 nAChR selective quinuclidine containing ligands with nanomolar affinities. The interaction characteristics of the fragments and the parent compounds with AChBP were evaluated using an SPR biosensor assay. The data obtained from this direct binding assay correlated well with data from the reference radioligand displacement assay. Ligand efficiencies for different (structural) groups of fragments in the library were correlated to binding with distinct regions of the binding pocket, thereby identifying ligand efficiency hot spots (LE hot spots). These hot spots can be used to identity the most promising hit fragments in a large scale fragment library screen.

Introduction

Fragment-based drug discovery (FBDD[a]) has become a central part in modern medicinal chemistry, and an increasing number of fragment screening and optimization studies are being published.[1] As the initial focus of FBDD is on low molecular weight fragments, there is a great need for technologies that can measure the weak binding of a fragment to a protein target. Biophysical techniques such as NMR spectroscopy, X-ray crystallography, mass spectrometry, and surface plasmon resonance (SPR biosensors) are particularly suited.[2−6] These assays do not require labeling of the ligand or protein, as is the case for displacement of radiolabeled or fluorescent ligands.

In the search for new compounds interacting with ligand-gated ion channels (LGIC), we are implementing fragment-based approaches. The LGICs of our interest are the nicotinic acetylcholine receptors (nAChRs) of the subgroup of Cys-loop receptors, also including the $GABA_A$ receptors, 5-HT_3-serotonin receptors, and glycine receptors. Many different subtype nAChRs are present in the CNS, including the highly expressed α4β2 and α7 subtypes.[7] They are important drug targets for Alzheimer's disease, Parkinson's disease, and schizophrenia.[8,9] The development of subtype selective ligands is one of the major challenges in the area of nAChRs. However, many of the biophysical screening technologies that have been developed and used for interaction studies with water-soluble proteins are not readily available for the transmembrane LGICs. In recent years the soluble acetylcholine binding protein (AChBP) has been adopted as a structural and pharmacological homolog of the extracellular domain (ECD) of nAChRs; the ECD constitutes the ligand-binding domain.[10,11] AChBP displays comparable ligand pharmacology to the α7 nAChR in particular.[11,12] Next to nAChRs,[13] AChBP has been used as a molecular tool to study structural and ligand-binding properties of other LGICs, i.e., 5-HT_3,[14] GABA,[15] and glycine[16] receptors. AChBP is also fused to the transmembrane ion pore of 5-HT_3 and glycine receptors to form chimeric channels that are useful for studying binding sites, activation mechanisms, and the different states of LGICs.[17,18] Several AChBPs have been identified from various snail species, e.g., *Aplysia californica* (Ac) and *Lymnaea stagnalis* (Ls), that differ slightly in pharmacology.[19]

To develop nAChR directed compounds, we consider SPR biosensor analysis as suitable for our FBDD studies. It allows for sensitive and label-free detection of binding fragments.[3,20] By immobilization of AChBP on the chip surface, protein consumption is very low. An additional advantage of direct binding biosensor-based interaction assays is the potential

*To whom correspondence should be addressed. Phone: +31-(0)20-5987841. Fax: +31-(0)20-5987610. E-mail: i.de.esch@few.vu.nl.

[a] Abbreviations: FBDD, fragment-based drug discovery; AChBP, acetylcholine binding protein; Ls, *Lymnaea stagnalis*; Ac, *Aplysia californica*; nAChR, nicotinic acetylcholine receptor; LGIC, ligand-gated ion channel; CNS, central nervous system; ECD, extracellular domain; SPR, surface plasmon resonance; RBA, radioligand binding assay; RU, response unit; LE, ligand efficiency; Tc-IFP, interaction fingerprint Tanimoto scores.

 Published on Web 09/09/2010

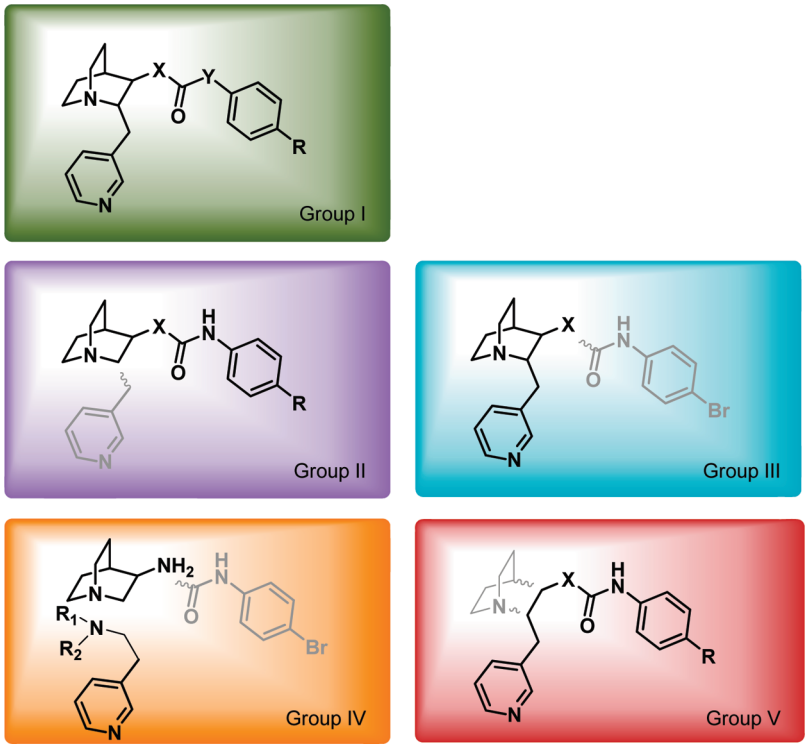

Figure 1. Generic structures of fragmentized quinuclidine compounds. Group I (green): high affinity α7 and AChBP compounds 2,3-disubstituted quinuclidines. Group II (purple): 3-substituted quinuclidines. Group III (aqua): 2,3-disubstituted quinuclidines with a truncated substituent in the 3 position. Group IV (orange): smaller fragments containing a basic amine. Group V (red): smaller fragments without a basic amine.

to identify orthosteric and ECD-bound allosteric compounds. The latter is of interest not only in the nAChRs field but also for other LGICs such as $GABA_A$[21] and 5-HT_3 receptors.[22] Earlier we have developed two biosensor-based assays: an indirect assay[23] (with bungarotoxin as displacement ligand) and a direct assay.[24] This direct assay is used and evaluated in the current paper.

Ideally, the technology used for fragment screening is able not only to identify the most promising hit fragment but also to guide efficient growing of these entities into bigger and more potent compounds. Here the ability of SPR biosensors to readily obtain kinetic and thermodynamic binding data can be a major advantage over traditional radioligand displacement assays.[25] An important concept for both fragment selection and fragment growing is ligand efficiency (LE).[26,27] LE indicates the contribution of the atoms in a compound to the affinity or activity and is defined as the binding energy divided by the molecular weight or number of heavy atoms of a ligand. Compounds with the highest LE are thought to have the highest potential to be optimized into potent leads. During the optimization process, LE is used to guide the efficient growing, linking, or merging of fragments into druglike molecules. In a hallmark paper by Hadjuk, a retrospective study indicated that LE ideally is maintained throughout the discovery process.[28] However, other studies, as well as an FBDD literature survey, indicate that LE is not always a constant factor during the fragment growing process.[1,29,30] Deconstruction of druglike molecules is an attractive tool to probe the binding energy contributions of ligand substructures to distinct areas and subpockets.[31−34]

We here present a deconstruction study of nAChR ligands. The primary aim of this deconstruction study is to benchmark the expectations of upcoming fragment hits with regard to ligand efficiencies (LE), enabling better evaluation in the fragment hit selection phase, as well as subsequent efficient fragment growing. In the process we want to validate our SPR biosensor assay[24] for fragment screening with AChBP. The obtained data are also used as a preliminary evaluation for the use of AChBP as molecular bait for nAChR ligands.

A set of α7 selective nAChR ligands was used to design and synthesize groups of fragments by deconstruction. To evaluate our SPR biosensor assay,[24] the SPR biosensor data for the fragment set were compared with the corresponding data obtained with the well established radioligand binding assay.[35] The data were generated with two different types of AChBP and compared with α7 nAChR affinity data. The affinity data for the fragments were used to calculate LEs. The LEs were projected on the surface of the binding pocket of Ls-AChBP using predicted binding modes, to identify potential "LE hot spots" in the pocket.

Results and Discussion

Ligand Deconstruction. A fragment set was designed from high-affinity quinuclidine-containing α7 receptor ligands (shown in green box in Figure 1, published by Mazurov et al.[36]). The similarity of α7 and AChBP ligand pharmacologies directed our choice for α7 selective ligands, while large ligands with high affinities were preferable to allow the synthesis of several groups of fragments with measurable affinities. These original ligands, with molecular weights of ~400 Da and nanomolar affinities, were included as druglike compounds representing the final products of a (fragment) hit optimization program (group I, Figure 1). Four groups of fragments were designed (groups II−V, Figure 1) covering molecular weights from 100 to 400 Da. A color scheme for

Scheme 1[a]

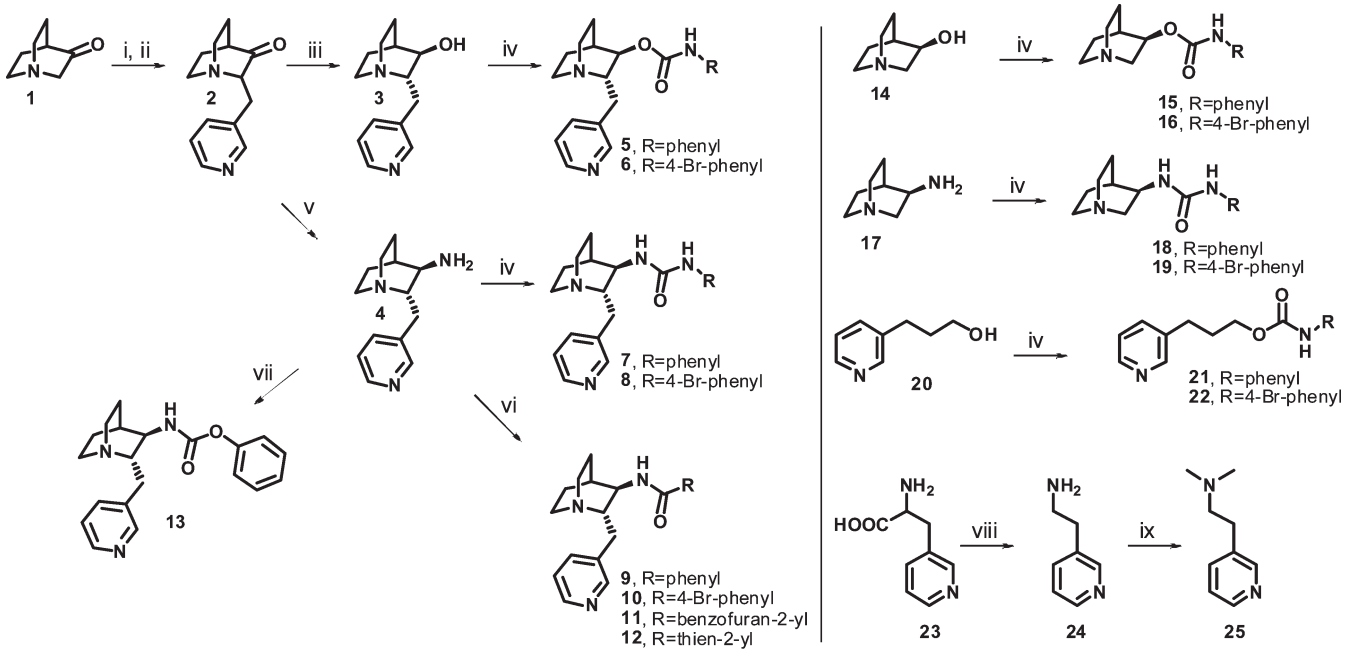

[a] Reagents and conditions: (i) 3-pyridinecarboxaldehyde, KOH, MeOH, reflux; (ii) H_2, Pd/C, MeOH, 3.45 bar, room temp; iii) $(i\text{-PrO})_3Al$, isopropanol, reflux; (iv) substituted isocyanates, triethylamine, DCM, room temp; (v) HCO_2NH_2, $NaCNBH_3$, $ZnCl_2$, MeOH, room temp; (vi) carboxylic acid, diphenylphosphoryl chloride, triethylamine, DCM, room temp; (vii) phenylchloroformate, triethylamine, DCM, room temp; (viii) dimethylaniline, 200 °C; (ix) formaldehyde, formic acid, reflux.

these groups is used consistently throughout the manuscript. Nicotine and an α7 selective nAChR ligand (**26**, PNU-282987[37]) were used as reference compounds.

Chemistry. The synthesis routes are given in Scheme 1. Compounds in groups I and III were synthesized from the commercially available quinuclidin-3-one (**1**) according to a literature procedure.[36] An aldol condensation with 3-pyridinaldehyde, followed by a reduction of the formed double bond and a reduction of the ketone to the corresponding alcohol with aluminum isopropoxide or to the corresponding amine with ammonium acetate and sodium cyanoborohydride, yielded **3** and **4**, respectively. For compounds in group II, amine **17** and the corresponding alcohol **14** were commercially available, as well as 3-(3-hydroxy)pyridine (**20**) for compounds in group V. Coupling with isocyanates gave the corresponding urea and carbamates. A peptide coupling with carboxylic acids gave the corresponding amides. Inverted carbamate **13** was synthesized by coupling **4** with phenylchloroformate. Fragments in group V were synthesized starting from 3-(3-pyridyl)-D-alanine (**23**): **24** was obtained by decarboxylation at high temperature,[38] and Eschweiler−Clarke methylation resulted in **25**.

Validation of SPR Biosensor Interaction Assay. Ls-AChBP and Ac-AChBP were immobilized to levels around 3000 RU. Higher amounts were avoided in order to reduce the effects of limited mass transport of analytes. Examples of sensorgrams are given for one representative compound per structural group (Figure 2). These examples show that high quality sensorgrams could be obtained for all fragment groups. Affinity values (K_D) could be determined for all compounds but not interaction rate constants due to very fast kinetics.[24] In some cases saturation could not be reached within the concentration range that could be reliably used.

The affinities of all 20 compounds for Ls-AChBP, along with nicotine and **26**, were determined in the SPR biosensor direct assay and radioligand displacement ([^{3}H]epibatidine) assay; affinities for α7-nAChR were determined in a radioligand displacement ([^{3}H]MLA) assay (Table 1). The affinities obtained for Ls-AChBP with the two assays were highly correlated ($R^2 = 0.97$), as shown in Figure 3A. This excellent correlation, for a diverse set of compounds with respect to molecular weight and affinities, between the novel SPR biosensor direct assay and the established radioligand displacement assay validates the quality of the SPR biosensor assay for the detection of binding of fragments.

The validity of AChBP as a model for α7-nAChR and the similarities of the binding sites were also evaluated by correlation analysis (Figure 3B,C). SPR biosensor affinity data (for Ls-AChBP in Figure 3B, for Ac-AChBP in Figure 3C) are correlated with α7-nAChR radioligand affinity data. The correlations between α7 and AChBP are quite low. Ls-AChBP data correlate better with the α7-nAChR data than the Ac-AChBP data, particularly for group I compounds. Therefore, our focus in the remainder of the article is on Ls-AChBP. In fact, two groups of fragments, group II (pink squares) and group III (blue triangles), show selectivity for either AChBP or α7. The group II urea and carbamates are better accommodated in the α7-nAChR, while group III 2-pyridine substituted quinuclidines have better interactions with Ls- and Ac-AChBP. This indicates significant differences between the binding sides of AChBP and the α7 receptor.

Ligand Efficiencies. The ligand efficiencies (LE) for all compounds were calculated from the experimentally determined ΔG values, using the (adjusted) formula of Hopkins et al.:[27] $LE = (\Delta G/MW) \times 1000$ (Table 1). Dividing by the molecular weight instead of the number of heavy atoms is more accurate in describing the difference between substituents with large molecular weight differences.[26] To monitor LE during the (retrospective) growth of low affinity fragments

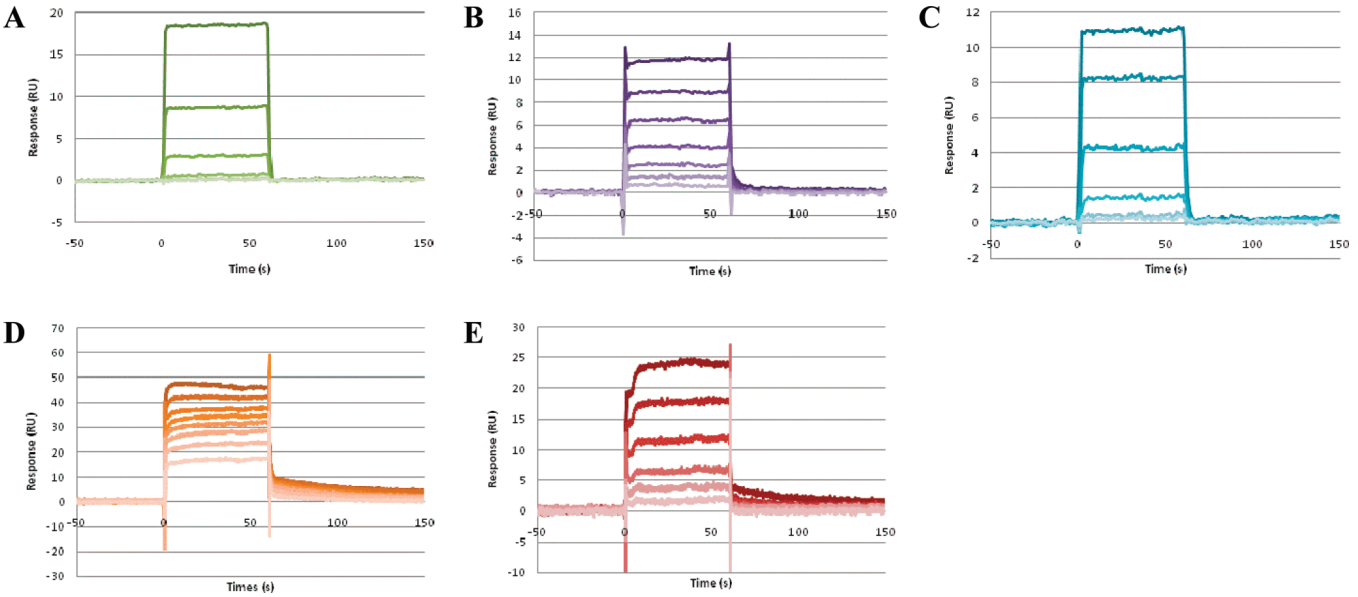

Figure 2. Examples of sensorgrams for one representative fragment from each group: (A) **8**, group I; (B) **17**, group II; (C) **3**, group III; (D) **25**, group IV; (E) **22**, group V.

into druglike compounds, LE is plotted against pK_i for Ls-AChBP (Figure 4A) and α7 nAChR (Figure 4B).

The focused fragment set gives insight into the contribution of the different parts of the quinuclidine compounds to binding. It is apparent that LEs differ remarkably for the different groups (Figure 4). The highest LEs are obtained for group IV fragments containing a basic nitrogen atom as part of a pyridine or amine group. Decoration of the quinuclidine 3-position leads to compounds with higher affinity but with significantly reduced LEs. Actually, for the majority of the compounds, the LE of the starting fragments (group IV, orange squares) is about twice as high as the LE of the "final" optimized compound (group I, green diamonds). Perhaps not surprisingly, the lowest LEs are found for the compounds in group V (red circles) that lack a basic nitrogen group. The basic center forms a cation under physiological conditions, and it is known that this charged group forms key cation−π interactions when binding to AChBP and nAChRs.[39]

When the LEs for the α7 nAChR are monitored, the trend is comparable with that for Ls-AChBP except for group II (purple stars) compounds (Figure 4B). The affinities of a majority of the compounds (groups I, III, IV, and V) are about 10 times higher for α7, but for three of the group II compounds the affinity is 100 times higher for α7. Urea **17** (group II) even has a LE of 39, which is higher than the group III compounds (while the group III compounds have lower LEs for α7 than for Ls). This illustrates that the binding region that accommodates the substituent in the 3-position of quinuclidine is more effectively addressed in the α7 nAChR than in AChBP. It is also noted that the dependency on the basic amine is greater for AChBP than for the α7 nAChR, as is suggested by the trend in the group V fragments.

Ligand Efficiency Hot Spots. Thus, from a retrospective growing consideration, the high LEs of the small fragments are not maintained in the optimized compounds. Following a typical fragment growing path (an example is shown in Figure 4), LE drops from 50 to 42 to 20 while affinity goes up with 2 log units. Apparently, certain parts of the molecule contribute much more to the binding energy and LE of the final ligand than others. To visualize this, we defined LE "hot parts" of a molecule and translate these parts to "LE hot spots" in the binding pocket. This is presented in Figure 5A−D, where docking modes of a representative compound of four fragment groups are presented.

Docking modes for the compound set were generated with Gold/Chemscore and ranked according to interaction fingerprint Tanimoto scores (Tc-IFP).[40] The binding mode of nicotine in the crystal structure of Ls-AChBP (1UW6) was used to generate the reference IFP. The use of IFP can easily overcome the imperfection of scoring functions with respect to induced fit,[41] since emphasis is given to important interactions known from available crystal structures. Comparison with experimental data from a crystal structure makes the resulting docking poses more reliable than using docking and scoring functions to select the best pose. Previously, we have used an induced-fit docking method to study flexibility of the loop regions upon ligand binding and as such addressed the dynamic process of ligand recognition.[24] The present docking studies with rigid protein as described here represent the end point of that process and the energy minimum as validated by X-ray analyses in which identical interactions are consistently present (i.e., pyridine nitrogen atoms of the ligands interact with a water molecule, etc.).

The LEs of the ligands are projected on the surface. The docking modes of **25**, **3**, and **8** (Figure 5A−C) indicate that a better resemblance of the nicotine binding mode yields a higher LE. Or in other words, the compound with the highest proportion of binding to the "hot spot" of the pocket gives the highest LE. Amine **25** (Figure 5A) makes all three important interactions that nicotine also makes in the crystal structure (Figure 5E), namely, (1) cation−π, mainly with aromatic side chain of Trp143, (2) a hydrogen bond with the backbone of Trp143, and (3) a hydrogen bond through a bridging water molecule (shown) to the main chain of residues Leu102 and Met114 (not shown). Quinuclidine **3** (Figure 5B) extends already in the direction of the cysteines, and the LE drops slightly. Ligand **8** (Figure 5C) extends further, whereas its LE drops to only 22 kcal·mol^{-1} Da^{-1}. Ligand **22** (Figure 5D) lacks a positive nitrogen and makes

Table 1. Structures and Affinities of All Compounds Determined by a Direct Binding Biosensor-Based Approach and an Indirect Radioligand Displacement Assay for Ls-AChBP, Ac-AChBP, and α7 nAChR[a]

Group/ Code	Structure	Biosensor		Radioligand Binding Assay			
		pK_D	pK_D	pK_i[1]	LE[2]	pK_i[3]	LE[2]
		Ls-AChBP	*Ac-AChBP*	*Ls-AChBP*	*Ls*	*α7*	*α7*
I	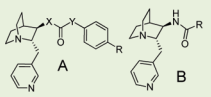 A B						
5	**A, X=O, Y=NH, R=H**	**7.00 ± 0.02**	**5.61 ± 0.06**	**7.21 ± 0.01**	**29**	**7.73 ± 0.02**	**31**
7	**A, X=NH, Y=NH, R=H**	**6.06 ± 0.01**	**4.71 ± 0.12**	**6.25 ± 0.17**	**26**	**7.54 ± 0.12**	**31**
6	**A, X=O, Y=NH, R=Br**	**7.62 ± 0.05**	**5.93 ± 0.16**	**7.74 ± 0.02**	**26**	**8.57 ± 0.09**	**28**
8	**A, X=NH, Y=NH, R=Br**	**6.36 ± 0.02**	**5.19 ± 0.07**	**6.15 ± 0.10**	**20**	**7.59 ± 0.12**	**25**
13	**A, X=NH, Y=O, R=H**	**6.46 ± 0.02**	**5.19 ± 0.09**	**6.30 ± 0.01**	**26**	**7.43 ± 0.05**	**30**
9	**B, R=phenyl**	**6.66 ± 0.04**	**5.12 ± 0.13**	**6.62 ± 0.02**	**28**	**7.21 ± 0.05**	**31**
10	**B, R=4-bromophenyl**	**7.03 ± 0.02**	**4.81 ± 0.08**	**7.05 ± 0.01**	**24**	**7.88 ± 0.01**	**27**
11	**B, R=benzofuran-2-yl**	**7.70 ± 0.01**	**5.29 ± 0.06**	**7.84 ± 0.02**	**30**	**8.56 ± 0.02**	**33**
12	**B, R=thien-2-yl**	**6.62 ± 0.01**	**4.79 ± 0.06**	**6.83 ± 0.02**	**29**	**7.36 ± 0.03**	**31**
II	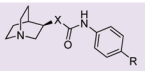						
15	**X=O, R=H**	**4.53 ± 0.05**	**4.24 ± 0.07**	**5.10 ± 0.06**	**28**	**5.71 ± 0.01**	**32**
16	**X=O, R=Br**	**5.35 ± 0.01**	**4.10 ± 0.05**	**5.52 ± 0.02**	**23**	**7.41 ± 0.01**	**31**
17	**X=NH, R=H**	**4.73 ± 0.02**	**3.74 ± 0.08**	**5.26 ± 0.02**	**29**	**6.96 ± 0.06**	**39**
18	**X=NH, R=Br**	**5.31 ± 0.03**	**4.48 ± 0.12**	**5.29 ± 0.03**	**22**	**7.36 ± 0.07**	**31**
III	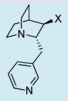						
3	**X=OH**	**6.50 ± 0.01**	**5.88 ± 0.03**	**6.60 ± 0.05**	**42**	**5.48 ± 0.07**	**35**
4	**X=NH_2**	**6.26 ± 0.02**	**5.13 ± 0.03**	**6.33 ± 0.04**	**40**	**5.64 ± 0.08**	**36**
IV	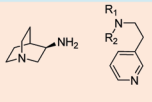 A B						
17	**A**	**4.13 ± 0.02**	**4.06 ± 0.05**	**3.96 ± 0.02**[4]	**51**	**5.20 ± 0.04**	**57**
24	**B, R_1=R_2=H**	**3.83 ± 0.07**	**3.12 ± 0.11**	**4.03 ± 0.08**[4]	**52**	**5.07 ± 0.09**	**57**
25	**B, R_1=R_2=Me**	**5.22 ± 0.04**	**3.87 ± 0.08**	**5.50 ± 0.02**	**50**	**5.50 ± 0.06**	**50**
V	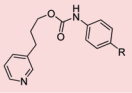						
21	**R=H**	**3.13 ± 0.13**	**2.68 ± 0.36**	**3.55 ± 0.02**[4]	**19**	**4.84 ± 0.13**	**26**
22	**R=Br**	**4.30 ± 0.10**	**3.50 ± 0.50**	**<5**	**18**[5]	**5.16 ± 0.08**	**21**
Nicotine		**6.32 ± 0.03**	**5.54 ± 0.15**	**6.48 ± 0.02**	**55**	**5.99 ± 0.03**	**51**
26	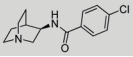	**5.44 ± 0.03**	**3.86 ± 0.14**	**5.68 ± 0.07**	**29**	**7.61 ± 0.02**	**39**

[a] (1) [^{3}H]MLA displacement. (2) Ligand efficiencies (LE) were calculated using the (adjusted) formula of Hopkins et al.:[27] LE = (ΔG/MW) × 1000. (3) [^{3}H]Epibatidine displacement. (4) Highest measured concentration: 10^{-3} M. (5) LE calculated using SPR biosensor determined pK_D.

only one interaction in the highest LE part of the pocket (the pyridine moiety with the conserved water molecule). Thus, its LE is even lower.

The identification of LE hot spots is relevant, as it allows for a more considered nomination of most promising fragment hits. For prioritization of the hits from a full fragment

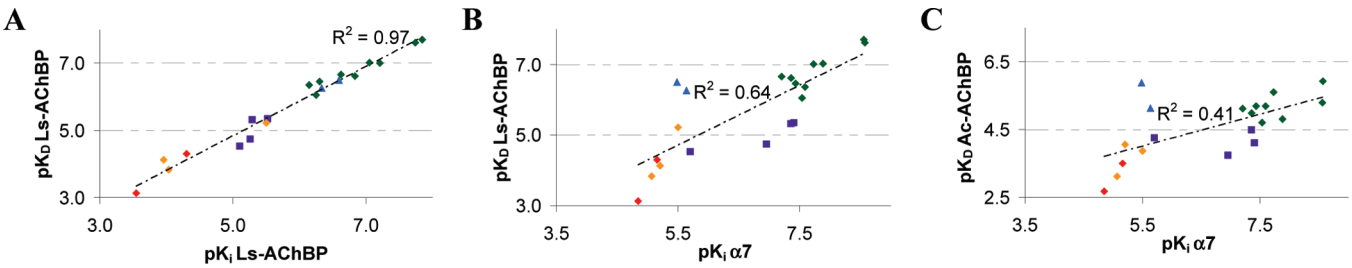

Figure 3. Comparison of the direct SPR data with radioligand displacement and AChBP with α7 data: (A) RBA pK_i versus SPR pK_D Ls-AChBP; (B) SPR pK_D data Ls-AChBP versus pK_i RBA α7; (C) SPR pK_D Ac-AChBP versus pK_i RBA α7.

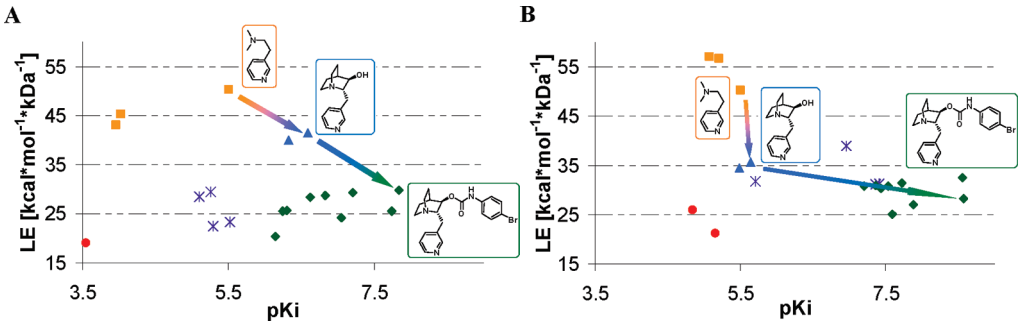

Figure 4. Monitoring ligand efficiency (LE) during (retrospective) fragment growing. Colors represent different groups: (A) Ls-AChBP data; (B) α7 nAChR data.

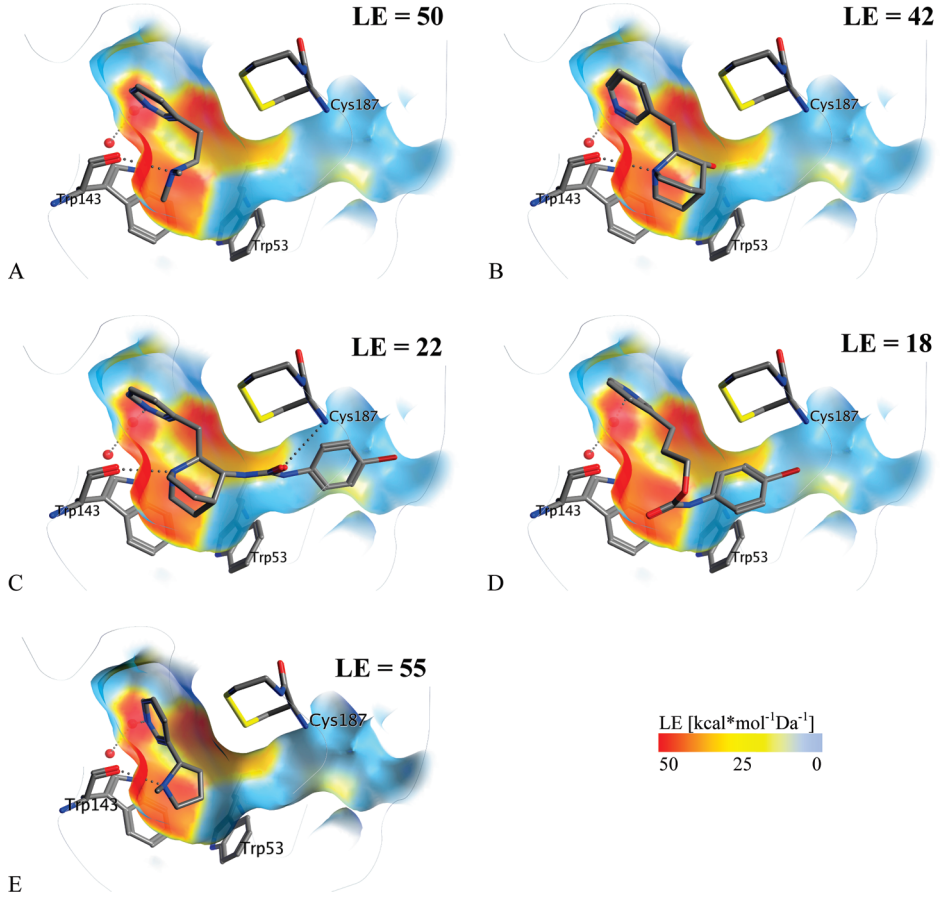

Figure 5. Docking modes in Ls-AChBP (1UW6) of (A) **25**, (B) **3**, (C) **8**, and (D) **22** and (E) crystal structure of nicotine in complex with Ls-AChBP. Ligand efficiencies were calculated from Ls-AChBP affinity data (RBA). The color coding of the surface was obtained by exchanging *B*-factors with LEs of ligands projected on protein atoms at 2.5 Å distances.

library screen, we intend to use a combination of predicted binding modes with weighting according to LE hot spots. For example, if hit fragments lacking a basic nitrogen atom have at least higher LEs than group V fragments (the

compounds lacking a cationic center as described in this study), the potential to develop these fragments into high affinity ligands by growing the core fragment toward the cation−π interaction site is considered as high.

Conclusion

Deconstruction of known α7 nAChR ligands has led to the identification of "LE hot spots". These hot spots are useful for evaluating the binding efficiency of fragments based on their LE. Fragments bound to these hot spots should have a very high LE, for growing will probably only decrease their LE. Fragments that bind to other areas than the LE hot spot can potentially be grown toward these hot spot, thereby increasing LE and affinity considerably.

We have used an SPR biosensor assay that is capable of detecting the binding of low molecular weight and low affinity fragments. SPR data are able to successfully guide fragment growing toward druglike and highly potent compounds. To our knowledge, the present SAR study based on SPR biosensor data for fragments is one of the first[2,3,20] in an emerging field and the data illustrate the use of SPR for fragment screening and optimization programs.

Experimental Section

Synthetic Methods. General Remarks. Chemicals and reagents were obtained from commercial suppliers and were used without further purification. The following compounds were purchased from Sigma-Aldrich: nicotine, **26**, and **17**. The following compounds were synthesized according to the literature:[36] **3**−**12**, **15**, **16**, **18**, **19**. The synthesis of **3** and **4** is described in detail because our chemical characterization (most notably through NMR analysis) identified the obtained material as the trans-isomers of the quinuclidines, whereas Mazurov et al. have reported the isolation of the cis-isomers in scientific literature. Very recently, however, the same group published different findings in the patent literature, where the isolated quinuclidine amines were indeed identified as the trans-isomers, as validated by X-ray analysis of the crystallized product.[42] Dry DCM and THF were obtained by distillation from $CaCO_3$. Flash column chromatography was typically carried out on a Biotage flash chromatography system, using prepacked Biotage Si columns with the UV detector operating at 254 nm. Analytical HPLC−MS analyses were conducted using a Shimadzu LC-8A preparative liquid chromatograph pump system with a Shimadzu SPD-10AV UV−vis detector with the MS detection performed with a Shimadzu LCMS-2010 liquid chromatograph mass spectrometer. Conditions were as follows: an Xbridge (C18) 5 μm column (100 mm × 4.6 mm) with solvent A (90% MeCN−10% buffer) and solvent B (90% water−10% buffer), flow rate of 1.0 mL/min, start 5% A, linear gradient to 100% A in 10 min, then 22.5 min at 90% A, then 12.5 min at 5% A, total run time of 45 min. The buffer is a 0.4% (w/v) NH_4CO_3 solution in water, adjusted to pH 8.0 with NH_4OH. Compound purities were calculated as the percentage peak area of the analyzed compound by UV detection at 254 nm. HRMS data were collected using a Bruker micrOTOF-Q (ESI). Purity and HRMS data for all compounds are listed in Supporting Information Table S1.

2-(Pyridin-3-ylmethyl)quinuclidin-3-ol (3). 2-(Pyridin-3-ylmethyl)quinuclidin-3-one (**2**, 2.5 g, 11.6 mmol) was dissolved in 35 mL of isopropanol. Aluminum *tert*-isopropoxide (7.1 g, 34.7 mmol) was added. The reaction mixture was refluxed for 6 h, concentrated, and dissolved again in water (100 mL) and dichloromethane (75 mL). The layers were separated; the water layer was extracted with dichloromethane (2 × 75 mL). The organic layer was dried with Na_2SO_4, filtered, and concentrated. An HCl salt was made of the product by stirring it in a saturated HCl solution in diethyl ether. A solid was formed and filtered. The product was recrystallized from acetone/methanol. Yield: 1.5 g (5.9 mmol, 51%). ^{1}H NMR (400 MHz, MeOD) δ (ppm) 8.59 (d, J = 1.81 Hz, 1H), 8.43 (dd, J = 4.89, 1.47 Hz, 1H), 7.98−7.86 (m, 1H), 7.42 (dd, J = 7.64, 4.70 Hz, 1H), 4.07−3.98 (m, 1H), 3.98−3.88 (m, 1H), 3.62−3.44 (m, 2H), 3.44−3.32 (m, 2H), 3.26−3.10 (m, 1H), 3.00 (dd, J = 13.77, 5.27 Hz, 1H), 2.37−2.25 (m, 1H), 2.25−2.17 (m, 1H), 2.07−1.94 (m, 1H), 1.94−1.69 (m, 2H). Absence of NOE signals between 2R and 3S protons confirmed trans-configuration (see Supporting Information for NOESY spectrum).

2-(Pyridin-3-ylmethyl)quinuclidin-3-amine (4). 2-(Pyridin-3-ylmethyl)quinuclidin-3-one (**2**, 18 g, 83 mmol) was dissolved in 900 mL of methanol. To this yellow solution, ammonium acetate (52.5 g, 0.83 mol) was added. The solution was stirred for 20 min at room temperature. Then $NaCNBH_3$ (19.3 g, 0.31 mol) and $ZnCl_2$ (1.13 g, 8.3 mmol) were added. The reaction mixture was stirred overnight at room temperature. The next day, another amount of $NaCNBH_3$ (0.5 equiv, 2.6 g, 41 mmol) was added. The reaction mixture was stirred for another 4 h, then concentrated and dissolved again in 1 M HCl solution until pH ∼6/7 was obtained. The mixture was washed with DCM (2 × 100 mL), then basified with 2.5 M NaOH to pH > 14. The water layer was extracted with DCM (3 × 200 mL). The organic layer was dried with Na_2SO_4, filtered, and concentrated. An HCl salt was made of the product by dissolving it in DCM and adding 2 M HCl solution in diethyl ether. The resulting solid was filtered and recrystallized from EtOH with 10% isopropanol. Yield: 4.6 g (14.7 mmol, 18%, 2.6 equiv of HCl). ^{1}H NMR (400 MHz, D_2O) δ (ppm) 8.82 (s, 1H), 8.72 (d, J = 5.62 Hz, 1H), 8.56 (d, J = 8.24 Hz, 1H), 8.00 (dd, J = 8.05, 5.75 Hz, 1H), 4.01 (dt, J = 10.74, 5.41 Hz, 1H), 3.72 (dd, J = 5.00, 2.54 Hz, 1H), 3.66−3.51 (m, 2H), 3.50−3.18 (m, 4H), 2.55−2.44 (m, 1H), 2.22−1.92 (m, 4H). Absence of NOE signals between 2R and 3S protons confirmed trans-configuration (see Supporting Information for NOESY spectrum).

Phenyl-2-(pyridine-3-ylmethyl)quinuclidin-3-ylcarbamate (13). The free base of **4** (0.5 g, 1.5 mmol) was dissolved in 5 mL of dry DCM and triethylamine (0.8 mL, 6.1 mmol). Phenylchloroformate (226 μL, 1.8 mmol) was added. The reaction mixture was stirred for 24 h and quenched with saturated $NaHCO_3$ solution (20 mL). This water layer was extracted with DCM (2 × 50 mL). The organic layer was dried with Na_2SO_4, filtered, and concentrated. The product was purified over SiO_2 (EtOAc 100%, TEA 2%, gradient to MeOH 20%), yielding 102 mg (0.30 mmol, 20%) of a white solid. ^{1}H NMR (400 MHz, CDCl3) δ (ppm) 8.54−8.36 (m, 2H), 7.54 (t, J = 9.69 Hz, 1H), 7.33 (t, J = 7.60 Hz, 2H), 7.18 (dd, J = 7.63, 4.81 Hz, 2H), 7.08 (dd, J = 14.35, 8.01 Hz, 2H), 5.86−5.67 (m, 1H), 3.49 (d, J = 6.73 Hz, 1H), 3.12−2.57 (m, 6H), 1.96 (s, 1H), 1.65 (s, 3H), 1.43 (t, J = 11.62 Hz, 1H). ^{13}C NMR (101 MHz, $CDCl_3$) δ 154.18, 150.98, 150.19, 147.44, 136.63, 135.00, 129.25, 125.25, 123.28, 121.52, 65.60, 55.14, 49.62, 40.84, 28.19, 26.27.

3-(Pyridine-3-yl)propyl phenylcarbamate (21). 3-Pyridinepropanol (**20**, 1 mL, 7.7 mmol) was dissolved in 25 mL of dry THF. Phenyl isocyanate (0.93 mL, 8.5 mmol) was added. The reaction mixture was stirred overnight at room temperature and then concentrated. Saturated $NaHCO_3$ solution was added (50 mL), and this water layer was extracted with DCM (2 × 50 mL). The organic layer was dried with Na_2SO_4, filtered, and concentrated. The product was purified over SiO_2 (EtOAc 100%, TEA 2%, gradient to MeOH 20%), yielding 1.58 g (6.2 mmol, 80%) of a white solid. ^{1}H NMR (400 MHz, CDCl3) δ (ppm) 8.45 (d, J = 5.68 Hz, 2H), 7.48 (d, J = 7.54 Hz, 1H), 7.39 (d, J = 7.55 Hz, 2H), 7.28 (t, J = 7.60 Hz, 2H), 7.23−7.14 (m, 1H), 7.04 (t, J = 7.22 Hz, 1H), 4.18 (t, J = 6.27 Hz, 2H), 2.69 (t, J = 7.69 Hz, 2H), 2.10−1.90 (m, 2H). ^{13}C NMR (101 MHz, $CDCl_3$) δ 153.67, 149.79, 147.50, 138.09, 136.60, 135.90, 129.03, 123.44, 123.39, 118.75, 64.12, 30.26, 29.38.

3-(Pyridine-3-yl)propyl 4-bromophenylcarbamate (22). 3-Pyridinepropanol (**20**, 1 mL, 7.7 mmol) was dissolved in 25 mL of dry THF. 4-Bromophenyl isocyanate (1.7 g, 8.5 mmol) was added. The reaction mixture was stirred overnight at room temperature and then concentrated. Saturated $NaHCO_3$ solution was added (50 mL), and this water layer was extracted with DCM (2 × 50 mL). The organic layer was dried with Na_2SO_4, filtered, and concentrated. The product was recrystallized from *tert*-butyl methyl ether/THF, yielding 0.71 g (2.1 mmol, 27%) of an off-white solid. ^{1}H NMR (500 MHz, DMSO) δ (ppm) 9.82 (s, 1H), 8.46 (d, J = 2.00 Hz, 1H), 8.41 (dd, J = 4.75, 1.58 Hz, 1H), 7.66 (dt, J = 7.80, 1.92 Hz, 1H), 7.50−7.39 (m, 4H), 7.32 (dd, J = 7.78, 4.76 Hz, 1H), 4.09 (t, J = 6.55 Hz, 2H), 2.75−2.66 (m, 2H), 2.01−1.90 (m, 2H). ^{13}C NMR (126 MHz, DMSO) δ 153.42, 149.57, 147.29, 138.61, 136.55, 135.79, 131.51, 123.48, 120.02, 113.88, 63.54, 29.74, 28.44.

2-(Pyridine-3-yl)ethanamine·HCl (24). 3-(3-Pyridyl)-D-alanine (**23**, 600 mg, 3.6 mmol) was stirred in 12 g of diphenylamine. This mixture was heated to 200 °C. When the formation of CO_2 gas was over (after 1 h), to the resulting yellow solution was added carefully 1 M HCl solution (50 mL). The mixture was cooled to room temperature and extracted with diethyl ether (6 × 50 mL). The organic layer was dried with Na_2SO_4, filtered, and concentrated to yield 309 mg (2.5 mmol, 70%) of the crude product, a yellow oil. An HCl salt was made with 4 M HCl in dioxane, and the product was recrystallized from ethanol, yielding 98 mg (0.50 mmol, 14%) of the double HCl salt, a white solid. ^{1}H NMR (500 MHz, DMSO) δ (ppm) 8.91 (s, 1H), 8.82 (d, J = 5.54 Hz, 1H), 8.55 (d, J = 8.04 Hz, 1H), 8.40 (s, 3H), 8.02 (dd, J = 7.96, 5.71 Hz, 1H), 3.18 (s, 4H). ^{13}C NMR (126 MHz, DMSO) δ 146.36, 142.07, 140.06, 137.47, 126.90, 38.73, 29.55.

***N,N*-Dimethyl-2-(pyridine-3-yl)ethanamine·HCl (25).** 2-(Pyridine-3-yl)ethanamine (**24**, 100 mg, 0.8 mmol) was refluxed in formaldehyde (2.5 mL of a 35 wt % solution in water/methanol) and formic acid (2.5 mL). After the mixture was cooled to room temperature, 10% NaOH solution (50 mL) was added and extracted with dichloromethane (3 × 50 mL). The organic layer was dried with Na_2SO_4, filtered, and concentrated. An HCl salt was made with 4 M HCl in dioxane, and the product was recrystallized from ethanol, yielding 66 mg (0.30 mmol, 37%) of the double HCl salt, a yellow solid. ^{1}H NMR (500 MHz, DMSO) δ (ppm) 11.17 (s, 1H), 8.94 (s, 1H), 8.83 (d, J = 5.43 Hz, 1H), 8.54 (d, J = 8.00 Hz, 1H), 8.02 (dd, J = 7.92, 5.69 Hz, 1H), 3.42 (s, 2H), 3.35−3.24 (m, 2H), 2.78 (d, J = 2.91 Hz, 6H). ^{13}C NMR (126 MHz, DMSO) δ 145.86, 142.17, 140.44, 137.01, 126.84, 55.75, 41.96, 26.48.

Protein Expression and Purification. His_6-*Lymnaea stagnalis*-acetylcholine binding protein (Ls-AChBP) and His_6-*Aplysia californa*-acetylcholine binding protein (Ac-AChBP) were expressed using the Bac-to-Bac baculovirus expression system (Invitrogen, Carlsbad, CA) following the manufacturer's recommendations. Secreted protein was trapped on an HIS-Select cartridge (Sigma, St. Louis, MO). The cartridge was washed with 24 mL of 10 mM imidazole, left overnight at 4 °C in 250 mM imidazole/Tris at pH 8, and thereafter eluted with 5 mL of 250 mM imidazole. A Slide-A-Lyzer dialysis cassette (Pierce, Rockford, IL) was used according to the manufacturer's recommendations to replace the imidazole by standard binding buffer. The purity of the protein was checked on an SDS gel, and the protein concentration was determined by Bradford analysis. Protein aliquots were stored at −80 °C until use. Human neuroblastoma cells (SH-SY5Y) expressing human α7 nAChRs were kindly provided by Christian Fuhrer (University of Zurich, Switzerland). Cells were washed with PBS, pelleted by centrifuging, and stored at −80 °C until use.

SPR Biosensor Assay. SPR biosensor experiments were performed at 25 °C on a BIAcore T100 (GE Healthcare, Uppsala, Sweden). Ls-AChBP and Ac-AChBP were diluted to 0.03−0.1 mg/mL in 50 mM NaAc (pH 5.5) and immobilized on a CM5 sensor chip (research grade, GE Healthcare, Uppsala, Sweden) by amine coupling according to the manufacturer's instructions. An unmodified dextran surface was used as a reference surface.

A phosphate buffer (10 mM phosphate, pH 7.0, 137 mM NaCl, 3 mM KCl, with addition of 5% DMSO and 0.005% v/v surfactant P20 (GE Healthcare, Uppsala, Sweden)) was used as a running buffer at a flow rate of 90 μL/min. All compounds were dissolved as 10 mM stock solutions in pure DMSO and diluted in the running buffer. Suitable concentration series were determined for all compounds separately. Typically, samples were injected for 60 s, and the dissociation was recorded for 300 s.

Signals were corrected for nonspecific binding to the surface by subtracting signals from the reference surface from those of the AChBP surfaces (reference subtraction). In addition, corrections for minor differences between AChBP and reference surface interactions with DMSO were performed by using a series of solvents standards (solvent correction). Moreover, signals were corrected for background by subtracting signals from a blank injection from those of compound injections (blank subtraction).

The affinity was determined by fitting a Langmuir binding equation to steady state binding signals at different concentrations. For the estimation of the affinity of compounds not reaching saturation within the range of concentrations that could be used for the measurements, the maximum binding level (R_{max}) was fixed to a value determined by a reference compound of similar molecular weight. Unless otherwise stated, standard deviations were based on at least four experimental series.

Radioligand Displacement Assay. For the radioligand displacement study, AChBP (Ls- or Ac-) was diluted in PBS-Tris binding buffer (final concentration of 1.4 mM KH_2PO_4, 4.3 mM Na_2HPO_4, 137 mM NaCl, 2.7 mM KCl, 20 mM Trizma base, 4% DMSO, 0.05% Tween 20, pH 7.4) to obtain a quantity of 1.3 ng per well. AChBP was incubated with 10^{-4}−10^{-11} M ligands (stock concentration of 10 mM in DMSO) in the presence of approximately 1.5 nM [^{3}H]epibatidine (K_D = 0.875 nM, Perkin-Elmer Life Scince, Inc.) and 0.2 mg of PVT Copper His-Tag SPA beads (GE Healthcare). For fragments with pK_i values below 4.5, AChBP was incubated with 10^{-3}−10^{-10} M solutions. Final well volume was 100 μL, and the incubation time was 60 min followed by 3 h in the dark. Thereafter, the label-bead complexes were counted in a micro-β-counter. Binding assays for the human α7 nAChR were performed in a similar way as described for AChBP. However, the cells with α7 nAChR were homogenized immediately for use and no PVT copper His-Tag SPA beads were added. As radioligand, ^{3}H-MLA (K_D = 1.81 nM, American Radiolabeled Chemicals, Inc.) was used at 2.5 nM. The binding assay data were analyzed using Prism 4.0 (Graphpad Software, Inc.).

Modeling. Compound Preparation. Three-dimensional structures were generated using MOE (version 2008.10, Chemical Computing Group, Montreal, Canada). In order to compare racemic compounds **3** and **8** with enantiopure *R*-isomer **17**, the 2*S*,3*R*-enantiomers were used in the docking experiments. Protonation was set such that strong acids and bases were charged. Partial atomic charges were calculated using Gasteiger charges, and the molecules were energy-minimized in vacuo using the MMFF94x force field in MOE.

Template Preparation. The Ls-AChBP crystal structure in complex with nicotine (PDB accession code 1uv6, 2.5 Å) and the Ac-AChBP crystal structure in complex with epibatidine (PDB accession code 2byq, 3.4 Å) were used for the generation of docking modes. The ligand and water molecules (except two conserved waters in Ls-AChBP in contact with nicotine) were removed, and hydrogen atoms were added to the protein models. Partial atomic charges were calculated, and energy-minimization was performed using the AMBER99 force field in MOE. The docking procedure was performed in one of the binding pockets formed by two adjacent subunits.

In Silico Docking Procedure. Docking studies were performed using the GOLD docking program (version 2.0)[43] and ChemScore and GoldScore scoring functions using default settings unless stated otherwise. For each ligand, 25 docking poses were calculated, allowing a cluster size of three ligands within a rmsd of 1.5 Å. Docking poses were chosen on the basis of their fitness score, ΔG score, and a pharmacophoric filter. This pharmacophoric filter consisted of the known interactions of nicotinic ligands, especially nicotine and epibatidine in their crystal structures, namely, cation$-\pi$ interaction, H-bond with Trp143 backbone, H-bond with conserved water. The pose with the highest amount of these interactions and the highest fitness score was chosen (see Table S2 in Supporting Information). In the case of **8** this corresponded to the pose with the highest ΔG; however, this pose scored lower because of higher clashes.

Interaction Fingerprint Scoring. Nicotine (in the Ls-AChBP X-ray structure) and epibatidine (in the Ac-AChBP X-ray structure) were used to generate reference interaction fingerprints (IFPs) as previously described.[40] Eight different interaction types (cation$-\pi$, negatively charged, positively charged, H-bond acceptor, H-bond donor, aromatic face-to-edge, aromatic face-to-face, and hydrophobic interactions) were used to define the IFP. The cavity used for the IFP analysis consisted of the 15 residues and 2 water molecules: Y89, S142, W143, T144, Y185, C187, C188, Y192, W53, L102, A103, R104, L112, Y113, M114, HOH1090, and HOH1045. Standard IFP scoring parameters[40] and a Tanimoto coefficient (Tc-IFP) measuring IFP similarity with the reference molecule pose were used to rank the docking poses generated with Gold/Goldscore and Chemscore. For the four docking poses in Figure 5, IFP, Goldscore, and Chemscore values are given in the Supporting Information Table S2.

LE Projection on Surface Maps. To visualize LEs of the ligands on the complementary surface of the binding pocket, protein atoms within 2.5 Å distance of a ligand were scored according to the LE of that ligand. The ligand with the highest LE was projected first (**25**). For the second ligand (**3**) additional contacts were scored according to $\Delta\Delta G/\Delta$MW (i.e., group efficiency[44]). This procedure was repeated for the third (**8**) ligand (**22**). These LE scores were stored in the PDB structure of Ls-AChBP as *B*-factors; the surface was subsequently colored by *B*-factors.

Acknowledgment. The authors thank Obbe Zuiderveld for conducting the radioligand displacement assay and Frans de Kanter for performing the NOESY experiments. K.R. was financially supported by Drug Discovery Center Amsterdam, G.E.d.K., A.B.S., and T.N. were financially supported within the framework of Top Institute Pharma Project No. D2-103. The research leading to these results has received funding from the European Union Seventh Framework Programme under Grant Agreement No. HEALTH-F2-2008-202088 ("NeuroCypres" project). M.G., A.B.S., and I.J.P.d.E were financially supported by NeuroCypres.

Supporting Information Available: Purity data, as determined by LC$-$MS, and exact masses, as determined by HRMS, for all compounds; NMR and NOESY spectra for **3** and **4**; and Gold, Chem, and IFP scores for relevant docking poses. This material is available free of charge via the Internet at http://pubs.acs.org.

References

(1) de Kloe, G. E.; Bailey, D.; Leurs, R.; de Esch, I. J. P. Transforming fragments into candidates: small becomes big in medicinal chemistry. *Drug Discovery Today* **2009**, *14*, 630–646.
(2) Danielson, U. H. Fragment library screening and lead characterization using SPR biosensors. *Curr. Top. Med. Chem.* **2009**, *9*, 1725–1735.
(3) Navratilova, I.; Hopkins, A. L. Fragment screening by surface plasmon resonance. *ACS Med. Chem. Lett.* **2010**, *1*, 44–48.
(4) Swayze, E. E.; Jefferson, E. A.; Sannes-Lowery, K. A.; Blyn, L. B.; Risen, L. M.; Arakawa, S.; Osgood, S. A.; Hofstadler, S. A.; Griffey, R. H. SAR by MS: a ligand based technique for drug lead discovery against structured RNA targets. *J. Med. Chem.* **2002**, *45*, 3816–3819.
(5) Nienaber, V. L.; Richardson, P. L.; Klighofer, V.; Bouska, J. J.; Giranda, V. L.; Greer, J. Discovering novel ligands for macromolecules using X-ray crystallographic screening. *Nat. Biotechnol.* **2000**, *18*, 1105–1108.
(6) Fesik, S. W.; Shuker, S. B.; Hajduk, P. J.; Meadows, R. P. SAR by NMR: an NMR-based approach for drug discovery. *Protein Eng.* **1997**, *10*, 73–73.
(7) Gotti, C.; Zoli, M.; Clementi, F. Brain nicotinic acetylcholine receptors: native subtypes and their relevance. *Trends Pharmacol. Sci.* **2006**, *27*, 482–491.
(8) Taly, A.; Corringer, P. J.; Guedin, D.; Lestage, P.; Changeux, J. P. Nicotinic receptors: allosteric transitions and therapeutic targets in the nervous system. *Nat. Rev. Drug Discovery* **2009**, *8*, 733–750.
(9) Jensen, A. A.; Frolund, B.; Lijefors, T.; Krogsgaard-Larsen, P. Neuronal nicotinic acetylcholine receptors: structural revelations, target identifications, and therapeutic inspirations. *J. Med. Chem.* **2005**, *48*, 4705–4745.
(10) Brejc, K.; van Dijk, W. J.; Klaassen, R. V.; Schuurmans, M.; van der Oost, J.; Smit, A. B.; Sixma, T. K. Crystal structure of an ACh-binding protein reveals the ligand-binding domain of nicotinic receptors. *Nature* **2001**, *411*, 269–276.
(11) Smit, A. B.; Syed, N. I.; Schaap, D.; van Minnen, J.; Klumperman, J.; Kits, K. S.; Lodder, H.; van der Schors, R. C.; van Elk, R.; Sorgedrager, B.; Brejc, K.; Sixma, T. K.; Geraerts, W. P. M. A glia-derived acetylcholine-binding protein that modulates synaptic transmission. *Nature* **2001**, *411*, 261–268.
(12) Hansen, S. B.; Radic, Z.; Talley, T. T.; Molles, B. E.; Deerinck, T.; Tsigelny, I.; Taylor, P. Tryptophan fluorescence reveals conformational changes in the acetylcholine binding protein. *J. Biol. Chem.* **2002**, *277*, 41299–41302.
(13) Grutter, T.; Le Novere, N.; Changeux, J. P. Rational understanding of nicotinic receptors drug binding. *Curr. Top. Med. Chem.* **2004**, *4*, 645–650.
(14) Thompson, A. J.; Lummis, S. C. R. 5-HT3 receptors. *Curr. Pharm. Des.* **2006**, *12*, 3615–3630.
(15) Ernst, M.; Bruckner, S.; Boresch, S.; Sieghart, W. Comparative models of GABA(A) receptor extracellular and transmembrane domains: important insights in pharmacology and function. *Mol. Pharmacol.* **2005**, *68*, 1291–1300.
(16) Chen, Z. L.; Dillon, G. H.; Huang, R. Q. Molecular determinants of proton modulation of glycine receptors. *J. Biol. Chem.* **2004**, *279*, 876–883.
(17) Grutter, T.; de Carvalho, L. P.; Dufresne, V.; Taly, A.; Fischer, M.; Changeux, J. P. A chimera encoding the fusion of an acetylcholine-binding protein to an ion channel is stabilized in a state close to the desensitized form of ligand-gated ion channels. *C. R. Biol.* **2005**, *328*, 223–234.
(18) Paulo, J. A.; Hawrot, E. Effect of homologous serotonin receptor loop substitutions on the heterologous expression in Pichia of a chimeric acetylcholine-binding protein with alpha-bungarotoxin-binding activity. *Protein Expression Purif.* **2009**, *67*, 76–81.
(19) Hansen, S. B.; Talley, T. T.; Radic, Z.; Taylor, P. Structural and ligand recognition characteristics of an acetylcholine-binding protein from *Aplysia californica*. *J. Biol. Chem.* **2004**, *279*, 24197–24202.
(20) Nordstrom, H.; Gossas, T.; Hamalainen, M.; Kallblad, P.; Nystrom, S.; Wallberg, H.; Danielson, U. H. Identification of MMP-12 inhibitors by using biosensor-based screening of a fragment library. *J. Med. Chem.* **2008**, *51*, 3449–3459.
(21) Sieghart, W. GABA(A) receptors as targets for different classes of drugs. *Drugs Future* **2006**, *31*, 685–694.
(22) Thompson, A. J.; Lummis, S. C. R. The 5-HT3 receptor as a therapeutic target. *Expert Opin. Ther. Targets* **2007**, *11*, 527–540.
(23) Retra, K.; Geitmann, M.; Kool, J.; Smit, G.; de Esch, I. J. P.; Danielson, U. H.; Irth, H. Development of SPR biosensor assays for primary and secondary screening of AChBP ligands. *Anal. Biochem.* [Online early access]. DOI: 10.1016/j.ab.2010.06.021. Published Online: June 17, 2010.
(24) Geitmann, M.; Retra, K.; De Kloe, G. E.; Homan, E.; Smit, A. B.; Esch, I. J. P.; Danielson, U. H. Interaction kinetic and structural dynamic analysis of ligand binding to acetylcholine-binding protein. *Biochemistry* [Online early access]. DOI: 10.1021/bi1006354. Published Online: August 12, 2010.
(25) Danielson, U. H. Integrating surface plasmon resonance biosensor-based interaction kinetic analyses into the lead discovery and optimization process. *Future Med. Chem.* **2009**, *1*, 1399–1414.
(26) Abad-Zapatero, C.; Metz, J. T. Ligand efficiency indices as guideposts for drug discovery. *Drug Discovery Today* **2005**, *10*, 464–469.
(27) Hopkins, A. L.; Groom, C. R.; Alex, A. Ligand efficiency: a useful metric for lead selection. *Drug Discovery Today* **2004**, *9*, 430–431.

(28) Hajduk, P. J. Fragment-based drug design: How big is too big? *J. Med. Chem.* **2006**, *49*, 6972–6976.
(29) Kuntz, I. D.; Chen, K.; Sharp, K. A.; Kollman, P. A. The maximal affinity of ligands. *Proc. Natl. Acad. Sci. U.S.A.* **1999**, *96*, 9997–10002.
(30) Reynolds, C. H.; Tounge, B. A.; Bembenek, S. D. Ligand binding efficiency: trends, physical basis, and implications. *J. Med. Chem.* **2008**, *51*, 2432–2438.
(31) Bissantz, C.; Kuhn, B.; Stahl, M. A medicinal chemist's guide to molecular interactions. *J. Med. Chem.* **2010**, *53*, 5061–5084.
(32) Hajduk, P. J. Puzzling through fragment-based drug design. *Nat. Chem. Biol.* **2006**, *2*, 658–659.
(33) Barelier, S.; Pons, J.; Marcillat, O.; Lancelin, J.-M.; Krimm, I. Fragment-based deconstruction of Bcl-xL inhibitors. *J. Med. Chem.* **2010**, *53*, 2577–2588.
(34) Brandt, P.; Geitmann, M.; Danielson, U. H. Deconstruction of non-nucleoside reverse transcriptase inhibitors of human immunodeficiency virus type-1 for exploration of the optimization landscape of fragments. Manuscript submitted.
(35) Ulens, C.; Akdemir, A.; Jongejan, A.; van Elk, R.; Bertrand, S.; Perrakis, A.; Leurs, R.; Smit, A. B.; Sixma, T. K.; Bertrand, D.; de Esch, I. J. P. Use of acetylcholine binding protein in the search for novel alpha 7 nicotinic receptor ligands. In silico docking, pharmacological screening, and X-ray analysis. *J. Med. Chem.* **2009**, *52*, 2372–2383.
(36) Mazurov, A.; Klucik, J.; Miao, L.; Phillips, T. Y.; Seamans, A.; Schmitt, J. D.; Hauser, T. A.; Johnson, R. T.; Miller, C. 2-(Arylmethyl)-3-substituted quinuclidines as selective alpha 7 nicotinic receptor ligands. *Bioorg. Med. Chem. Lett.* **2005**, *15*, 2073–2077.
(37) Bodnar, A. L.; Cortes-Burgos, L. A.; Cook, K. K.; Dinh, D. M.; Groppi, V. E.; Hajos, M.; Higdon, N. R.; Hoffmann, W. E.; Hurst, R. S.; Myers, J. K.; Rogers, B. N.; Wall, T. M.; Wolfe, M. L.; Wong, E. Discovery and structure−activity relationship of quinuclidine benzamides as agonists of alpha 7 nicotinic acetylcholine receptors. *J. Med. Chem.* **2005**, *48*, 905–908.
(38) Niemann, C.; Hays, J. T. The relation between structure and histamine-like activity. *J. Am. Chem. Soc.* **1942**, *64*, 2288–2289.
(39) Xiu, X. A.; Puskar, N. L.; Shanata, J. A. P.; Lester, H. A.; Dougherty, D. A. Nicotine binding to brain receptors requires a strong cation−pi interaction. *Nature* **2009**, *458*, 534–537.
(40) Marcou, G.; Rognan, D. Optimizing fragment and scaffold docking by use of molecular interaction fingerprints. *J. Chem. Inf. Model.* **2007**, *47*, 195–207.
(41) de Graaf, C.; Rognan, D. Selective structure-based virtual screening for full and partial agonists of the beta 2 adrenergic receptor. *J. Med. Chem.* **2008**, *51*, 6620–6620 (correction to *J. Med. Chem.* **2008**, *51*, 4978−4985) .
(42) Bencherif, M. B.; Benson, L.; Dull, G. M.; Fedorov, N.; Gatto, G. J.; Genus, J.; Jordan, K. G.; Mathew, J.; Mazurov, A. A.; Miao, L.; Munoz, J. A.; Pfeiffer, I.; Pfeiffer, S.; Phillips, T. Y. (2*S*,3*R*)-*N*-(2-((3-Pyridinyl)methyl)-1-azabicyclo[2.2.2]oct-3-yl-benzyofuran-2-carboxamide, novel salt forms, and methods of use thereof. U.S. Patent Application 20090048290, 2008.
(43) Jones, G.; Willett, P.; Glen, R. C.; Leach, A. R.; Taylor, R. Development and validation of a genetic algorithm for flexible docking. *J. Mol. Biol.* **1997**, *267*, 727–748.
(44) Verdonk, M. L.; Rees, D. C. Group efficiency: a guideline for hits-to-leads chemistry. *ChemMedChem* **2008**, *3*, 1179–1180.